Molecular Crystals and Liquid Crystals

Publication details, including instructions for authors and subscription information:
http://www.tandfonline.com/loi/gmcl20

Ferroelectric Liquid Crystal Based Tunable Microspectrometer

John W. McMurdy [a], Gregory P. Crawford [a] & Gregory D. Jay [b]

[a] Division of Engineering, Box D, Brown University, Providence, RI, USA

[b] Department of Emergency Medicine, Rhode Island Hospital, Providence, RI, USA

Version of record first published: 22 Sep 2010

To cite this article: John W. McMurdy, Gregory P. Crawford & Gregory D. Jay (2007): Ferroelectric Liquid Crystal Based Tunable Microspectrometer, Molecular Crystals and Liquid Crystals, 476:1, 61/[307]-76/[322]

To link to this article: http://dx.doi.org/10.1080/15421400701681034

Mol. Cryst. Liq. Cryst., Vol. 476, pp. 61/[307]–76/[322], 2007

ISSN: 1542-1406 print/1563-5287 online
DOI: 10.1080/15421400701681034

Taylor & Francis
Taylor & Francis Group

Ferroelectric Liquid Crystal Based Tunable Microspectrometer

John W. McMurdy
Gregory P. Crawford
Division of Engineering, Box D, Brown University, Providence, RI, USA

Gregory D. Jay
Department of Emergency Medicine, Rhode Island Hospital, Providence, RI, USA

A notch filter with minimum reflection bandwidth <20 nm and thermally tunable throughout the visible regime is fabricated using vertically aligned deformed helix ferroelectric liquid crystals. The performance of this filter is characterized both experimentally and theoretically as a tunable Bragg reflection grating. The utility of the filter as a microspectrometer is assessed by recreating the emission spectra of a mercury arc lamp and a liquid crystal display. The recorded performance of the microspectrometer lends it to applications using lower resolution spectral analysis and requiring compact and inexpensive devices such as rapid on-line screening or as disposable sensors.

Keywords: ferroelectric liquid crystals; notch filter; spectroscopy; tunable photonic crystal

1. OBJECTIVE AND BACKGROUND

Applications utilizing visible regime spectroscopy include chemical analysis, structural evaluation, optical quality analyses, and tissue characterization. Conventional spectrometers require a system of lenses and moving parts or high-density focal plane arrays (FPA) for spectral decomposition, translating directly into larger and more

The authors wish to acknowledge James Eakin as well as financial support from the Charles E. Culpeper Biomedical Initiative Pilot Program and the NASA GSRP fellowship program.

Address correspondence to John McMurdy, Division of Engineering, Box D, Brown University, Providence, RI 02906, USA. E-mail: john_mcmurdy@brown.edu

costly instrumentation. Although micromachining techniques have reduced the size and cost of these devices, including compact fiber based spectrometers, they remain inhibitive in certain applications including rapid screening and quality control testing, disposable spectrometers for chemical analysis, or in compact biomedical sensors. Single chip microspectrometers having few components and no moving parts overcome limitations of grating/FPA spectrometers or scanning grating spectrometers, namely size and cost. Several efforts to fabricate such a device have been disclosed. Correia *et al.* has examined using an array of 16 fabry-perot etalons with varying cavity lengths coupled with CMOS detectors as a static microchip device [1]. While this device is easy to manufacture and customizable to suit application needs, it is limited to static notch filters detecting 16 discrete points and interpolating spectral signatures. Lammel *et al.* has fabricated a tunable optical filter based on a silicon Bragg grating and a micro-actuator modulate the angle of the Bragg grating, achieving a resolution of 20 nm [2]. A spectrally sensitive monolithic device has also been proposed by creating a spatial interference pattern on an FPA and then Fourier transforming (FT) the signal recreates the incident spectrum [3]. This embodiment is attractive for its simple and passive design, although the resolution is directly correlated the interferogram monitoring FPA pixel density. Numerous other similar approaches have been made at microspectrometers based on FT techniques [4–6]. Other more traditional miniature monolithic devices have also been evaluated using phase transmission gratings coupled with an FPA [7] as well as alternative methods of manufacturing self focusing micro-gratings using deep etching x-ray lithography [8].

Liquid crystal (LC) materials are an interesting choice for microspectrometer applications due to their optical anisotropy and responsivity to both applied fields and thermal energy. Liquid crystal materials aligned in different morphologies enable devices with an optical reflection notch which may be tuned or deactivated with applied voltage, two of which include holographically formed polymer dispersed liquid crystals (H-PDLC's) or cholesteric liquid crystals (CLC's). CLC materials have been utilized in reflective display applications in a notch activated/deactivate fashion [9] as well as other applications in which the peak reflection wavelength may be tuned using in-plane electrodes; [10] however the wide bandwidth of the reflection notch (FWHM $\sim$ 70 nm) coupled with the polarization sensitivity in reflection (reflects only one circular polarization state) make these materials less than ideal for microspectrometer applications. H-PDLC's, which have also been explored as reflective displays [11]

and as color separation devices [12], have the advantage of a narrow bandgap in the transmission spectra (FWHM $\sim$ 15 nm) making the technology more applicable for a microspectrometer application, however, these devices have only shown a tunability of 15 nm in a single panel and concomitantly require multiple panels to achieve full visible spectral coverage. We propose the use of vertically aligned deformed helix ferroelectric liquid crystals (VA-DHFLC), a technology coupling the full spectrum tunability of a cholesteric liquid crystal with the narrow bandgap reflection notch ($<$20 nm) and relative polarization insensitivity of an H-PDLC Bragg reflection grating.

The intrinsic properties of DHFLC's have been exploited in numerous other applications, the majority of which use electric fields to drive the ferroelectric liquid crystal (FLC) alignment to one side of the conic structure. VA-DHFLC materials have been implemented in a waveplate configuration such that the waveplate axis is manipulated using circularly patterned in-plane electrodes to modulate FLC alignment [13]. VA-DHFLC's also have been shown to function as intrinsic and tunable feedback mechanism in a laser cavity and, when doped with fluorescent dyes, enable mirrorless lasing [14]. DHFLC's act as rapid cavity resonance modulators in fabry-perot etalons, enabling rapid tuning of etalon transmission properties [15] while similar properties have been applied in dynamic FLC holograms in WDM optical networks [16]. The literature also shows numerous configurations of DHFLCs being used in liquid crystal display technology. One novel method uses a VA-DHFLC sandwiched between a single linear polarizer and $\lambda/2$ waveplate/metallic reflector stack [17]. In-plane electrodes generate an electric field that is sufficiently strong to remove the DHFLC pitch and force the initially average isotropic cell to become anisotropic and modulate pixel output. Short pitch FLC's as well have shown promise in a polymer dispersed configuration, denoted polymer dispersed ferroelectric liquid crystals (PDFLC's), creating a bandgap structure analogous to an H-PDLC [18,19]. The permanent dipole of the FLC material in the PDFLC overcomes slow switching times inherent in more conventional polymer dispersed liquid crystal devices; however the tunability is still small and limited by the finite birefringence values is not suitable for monolithic microspectrometers. Using a single panel VA-DHFLC cell as a microspectrometer is a new concept and well suited due the optical and electrical properties of these materials. A VA-DHFLC microspectrometer has no moving components, actively scans spectral features using applied fields or temperature, and requires only a single pixel photodiode, making it ultra-compact, inexpensive, and easy to manufacture.

2. THEORY OF OPERATION

A DHFLC aligned vertically between two substrates can be treated as grating structure and the grating characterization parameter, Q, given in equation (1) can be used to describe it where λ is the wavelength of incident light, d is the grating thickness, and Λ is the grating pitch.

$$Q = 2\pi \frac{\lambda d}{n\Lambda^2} \tag{1}$$

For cases when $Q \ll 1$, the cell behaves in the Raman Nath regime; however in the case of short pitch FLC materials, Λ is on the order of λ and thus $Q \gg 1$ causing the grating to behave in the Bragg regime. In the vertically aligned condition, the Bragg planes will be mostly perpendicular to the substrate normal and operate in a coherent reflection mode dependent on index profile. This configuration is shown in Figure 1. In the case of the vertically aligned condition, the index profile of a VA-DHFLC cell for every incident polarization state as a function of the depth z and the incidence angle can be represented by the equation:

$$n(z, \theta_{\text{inc}}) = n_{\text{avg}}(\theta_{\text{inc}}) + n_m(\theta_{\text{inc}}) \cos(K(\theta_{\text{inc}})z) \tag{2}$$

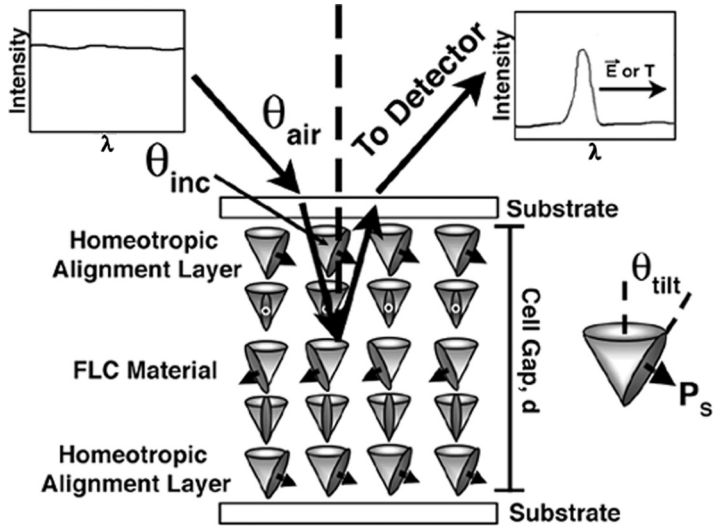

FIGURE 1 Configuration of a vertically aligned deformed helix ferroelectric liquid crystal cell operating in the reflective mode.

where n_{avg} is the average index as a function of θ_{inc}, the angle between the FLC helical director and the incident wavevector, n_{m} is the index modulation as a function of θ_{inc}, and $K = 2\pi/\Lambda$ is also a function of θ_{inc}. Using the standard equation describing the average index in a liquid crystal

$$\frac{1}{n_{\text{avg}}^2} = \frac{\cos^2(\theta_{\text{tilt}})}{n_0^2} + \frac{\sin^2(\theta_{\text{tilt}})}{n_e^2} \tag{3}$$

where θ_{tilt} is the tilt angle of the liquid crystal molecule, n_0 is the ordinary index and n_{e} is the extraordinary index, the VA-DHFLC spectral performance can be modeled. Manipulating equation (3) for a FLC configuration, the effective birefringence Δn_{eff} experienced by each polarization state propagating through the VA-DHFLC cell can be written as a function of the DHFLC tilt angle, θ_{tilt}, angle of incidence between helical director and incident wavevector (in the liquid crystal), θ_{inc}, and ordinary and extraordinary index of the FLC material, n_0 and n_{e}.

$$\begin{aligned}
\Delta n_{\text{eff}} &= \sqrt{\frac{1}{\left(\frac{\cos^2(\theta_{\text{tilt}}+\theta_{\text{inc}})}{n_o^2}\right) + \left(\frac{\sin^2(\theta_{\text{tilt}}+\theta_{\text{inc}})}{n_e^2}\right)}} - n_o, \quad \theta_{\text{inc}} < \theta_{\text{tilt}} \\
\Delta n_{\text{eff}} &= \sqrt{\frac{1}{\left(\frac{\cos^2(\theta_{\text{tilt}}+\theta_{\text{inc}})}{n_o^2}\right) + \left(\frac{\sin^2(\theta_{\text{tilt}}+\theta_{\text{inc}})}{n_e^2}\right)}} \\
&\quad - \sqrt{\frac{1}{\left(\frac{\cos^2(\theta_{\text{tilt}}-\theta_{\text{inc}})}{n_o^2}\right) + \left(\frac{\sin^2(\theta_{\text{tilt}}-\theta_{\text{inc}})}{n_e^2}\right)}}, \quad \theta_{\text{inc}} > \theta_{\text{tilt}}
\end{aligned} \tag{4}$$

Plotting Eq. (4) as a function of incidence angle for several FLC tilt angles, the effective birefringence value is maximized at $\theta_{\text{inc}} = 45^\circ$ when $\theta_{\text{inc}} < \theta_{\text{tilt}}$. The effective birefringence achieves its maximum value ($\Delta n_{\text{eff}} = \Delta n_{\text{flc}}$) at $\theta_{\text{tilt}} = 45^\circ$ and $\theta_{\text{inc}} = 45^\circ$. The effective birefringence maximum is maintained $\theta_{\text{tilt}} > 45^\circ$ by decreasing the incidence angle. Minimum effective birefringence is seen at normal incidence (of all feasible $\theta_{\text{inc}} < 80^\circ$) because the effective birefringence is much lower than that of the liquid crystal molecule ($\Delta n_{\text{eff}} \ll \Delta n_{\text{flc}}$). Figure 2 shows the modeled normalized effective birefringence as a function of θ_{tilt} and θ_{inc} as described by Eq. (4).

The reflection efficiency, ε, is determined by treating the VA-DHFLC cell as a volume phase grating and using a simplified version of the phase grating reflection efficiency equation as is shown in Eq. (5) [20].

$$\varepsilon(\theta_{\text{inc}}) = \tanh^2\left(\frac{\pi\Delta n_{\text{eff}}(\theta_{\text{inc}})d}{2\lambda_0}\right) \tag{5}$$

where d is the cell thickness and λ_0 is the reflected peak center wavelength. It is noted that the reflection efficiency variation with reflection notch wavelength is considered purely as a function of the number of Bragg planes while dispersion and birefringence modulation with decreasing order parameter are excluded in this equation. For a microspectrometer, the bandwidth of the reflection notch should be minimized while maximizing the reflection notch depth. The bandwidth of the cell, given in Eq. (6) from that of a Bragg reflection grating, shows that a while increasing the effective birefringence increases the peak reflectance, it also increases the reflectance bandwidth.

$$\Delta\lambda_{\text{refl}}(\theta_{\text{inc}}) = \lambda_0\Delta n_{\text{eff}}(\theta_{\text{inc}}) \tag{6}$$

The trade off between peak reflectance and reflection bandwidth is important when designing a DHFLC cell as a microspectrometer. Equations (4–6) and the material properties of the ferroelectric liquid crystal can be used to model the reflection spectra of a VA-DHFLC as a function of peak reflection wavelength and device orientation as is presented in Section 4.

3. METHODS

3.1. DHFLC Cell Fabrication

Cells were constructed for temperature regulated pitch modulation. Thermally tunable VA-DHFLC samples were prepared using Nissan SE-120 polyimide (Brewer Science Ltd) spin-coated on glass substrates. The polyimide was chosen because it promoted homeotropic alignment of liquid crystals. The polyimide layer was first spin-coated at 3000 rpm for 30 seconds to achieve a layers thickness of $\sim$200 nm. Following the spin-coating, the polyimide was processed by heating on a hotplate at 100°C for 10 minutes to remove the solvent followed by an imidization in an oven at 180°C for 90 minutes. Empty cells were constructed using two pieces of the polyimide coated glass having a constant cell gap of 10 μm maintained by glass fiber spacers. The larger cell gap and consequent improved reflection efficiency is enabled by operating the device in the thermal mode. Commercially available deformed helix ferroelectric liquid crystal material (ROLIC 10855, *Rolic Research*, Allschwil, Switzerland) with a pitch length $<$200 nm at room temperature, a spontaneous polarization (P_s) of 98 nC/cm^2,

a tilt angle (θ_{tilt}) of 38°, a birefringence (Δn_{flc}) of 0.07 at 550 nm, and phase sequence of Smectic C*/FLC < 83°C < Nematic* < 93°C < Isotropic. The DHFLC was capillary filled into the empty cell under a vacuum in the isotropic phase and cooled to room temperature under ambient conditions. The cell was then sealed with UV epoxy and cured to maintain stability. Electrically tunable cells can be fabricated similarly to thermally tunable cells except one substrate is coated with indium-tin-oxide (ITO) prior to coating with polyimide varnish. While this configuration is capable of tuning the spectral reflection of a VA-DHFLC using applied field, thermal modulation will be addressed here while in-plane electrode driving will be reported in a future disclosure.

3.2. VA-DHFLC Properties

Thermal tuning was performed using a contact resistive heating stage with a 0.5°C resolution (Instec, Boulder, CO). To investigate reflection notch characteristics when operating in thermal mode, the DHFLC cell was mounted on the heating stage and illuminated with a broadband white light halogen source. Reflection spectra from the VA-DHFLC were collected using a visible/near infrared grating spectrometer (USB2000, Ocean Optics, Dunedin, FL) with 4 nm resolution and operating range from 330 nm to 1030 nm. The cell was tuned from 50–83°C to fully examine the dynamic range of the sample before crossing the FLC-Nematic* phase transition point and disrupting the helical configuration. The cell was oriented at an incidence angle in air, θ_{air}, of 45° with respect to the collimated halogen source to demonstrate the full visible/NIR spectral range of tunability. The experimentally determined reflection characteristics are then compared to the results of the model in Section 2 treating the VA-DHFLC as a Bragg reflection grating with angular-dependent birefringence and subsequent peak reflection and bandwidth. Using the FLC material with birefringence $\Delta n = 0.07$, tilt angle $\theta_{\text{tilt}} = 38^\circ$, and orienting with $\theta_{\text{air}} = 45^\circ$ ($\theta_{\text{inc}} = 28.1^\circ$ as a result of refraction at substrates), Eq. (4) is used to derive the index modulation in the Bragg grating. The index modulation is then used in Eqs. (5) and (6) to determine maximum reflectivity and bandwidth. Several Gaussian reflection spectra with central reflection wavelength corresponding to experimentally recorded data were plotted using model-determined parameters. The modeled data was also plotted with orientation $\theta_{\text{air}} = 10^\circ$ ($\theta_{\text{inc}} = 6.8^\circ$) to highlight the angular dependent resolution of these samples.

The angular sensitivity was verified by monitoring the transmission of the VA-DHFLC cell as a function of the incidence angle

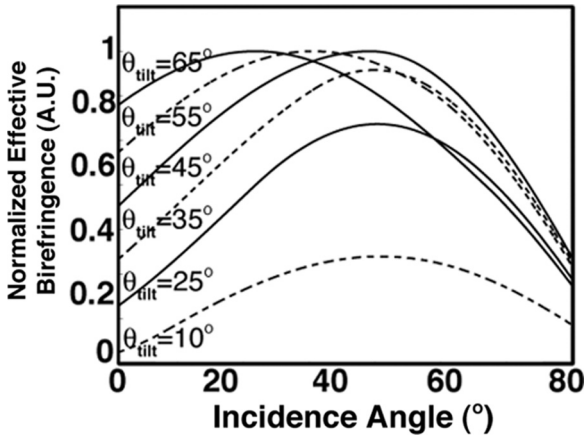

FIGURE 2 Modeled determined effective birefringence as a function of the tilt angle θ_{tilt} of the ferroelectric liquid crystal and the angle of incidence θ_{inc} with respect to the normal.

again using a grating spectrometer and collimated broadband source. The VA-DHFLC cell was placed on a rotational heating stage and heated to 65°C inducing a reflection notch at 550 nm. Transmission spectra were analyzed in this case to eliminate small variability in alignment while adjusting setup for different geometrical configuration. Transmission spectra were monitored as a function of θ_{air} from 10° to 50° (θ_{inc} from 6.8° and 30.7°); below $\theta_{\text{air}} = 10°$ the effective birefringence was sufficiently small causing minimal Bragg reflection and above $\theta_{\text{air}} = 50°$ the overall transmission signal was weak due to the reduced size of the VA-DHFLC clear aperture and initial waveguide losses in transmission mode.

Lastly, the polarization sensitivity of the DHFLC cell was characterized by monitoring the reflected intensity for both right and left handed circularly polarized light from a 532 Argon Ion Laser (Coherent, Santa Clara, CA). The cell was thermally tuned to a center reflection maximum of 532 nm (to correspond to the laser emission maxima) and a fiber spectrometer was used to measure the reflected emission intensity while rotating a 532 nm quarter waveplate by 90°.

3.3. Performance Characterization

The performance of a VA-DHFLC microspectrometer is assessed theoretically and experimentally. As reference emission standards, a liquid crystal display (LCD) and a mercury arc lamp were interrogated using

the microspectrometer device. The emission of both standards was first measured using the same grating spectrometer as above. Using these spectra, modeled reflection spectra of a VA-DHFLC device as determined using the method in section 2 with $\theta_{air} = 25^{\circ}$ were applied as weighting factors and then signals summed to simulate the incident power on a single pixel diode and emulate microspectrometer performance. The modeled microspectrometer performance was broken down into 350 discrete VA-DHFLC reflection notches ranging from 400 nm to 750 nm and the summed intensity from each notch was then recombined with its central wavelength to recreate the spectrum. To verify microspectrometer performance experimentally, the emission standards were focused onto a single pixel photodiode (Melles-Griot, Rochester, NY) using a high clear aperture lens after reflecting from the VA-DHFLC sample at an incidence angle $\theta_{air} = 25^{\circ}$ ($\theta_{inc} = 16.3^{\circ}$). The incidence angle was chosen at an angle to compromise high signal to noise with angular resolution dependence. The VA-DHFLC was thermally tuned from 50–83°C to cover the full visible regime at a rate of 3°C/min.

4. RESULTS

4.1. VA-DHFLC Properties

Reflection spectra of the VA-DHFLC as a function of temperature are shown in Figure 3(a). The reflection notch shifts from the UV regime (at room temperature) continuously through the short and long wavelength visible regime. Figure 3(b) shows the peak reflection

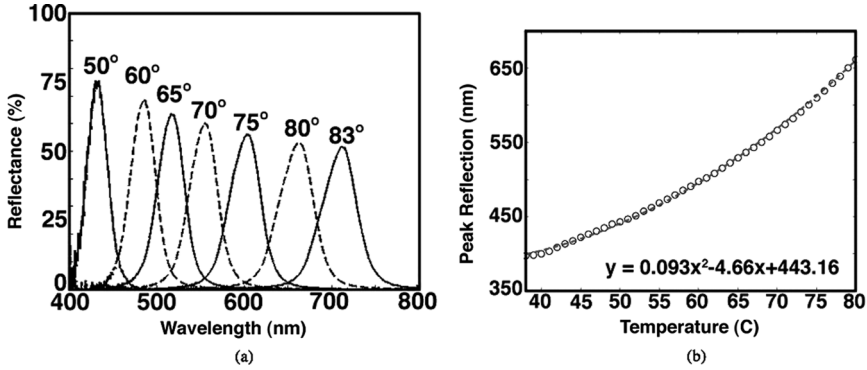

FIGURE 3 Reflection spectra of a 10 μm VA-DHFLC as a function of temperature (a) and the peak reflectance wavelength as a function of temperature (b).

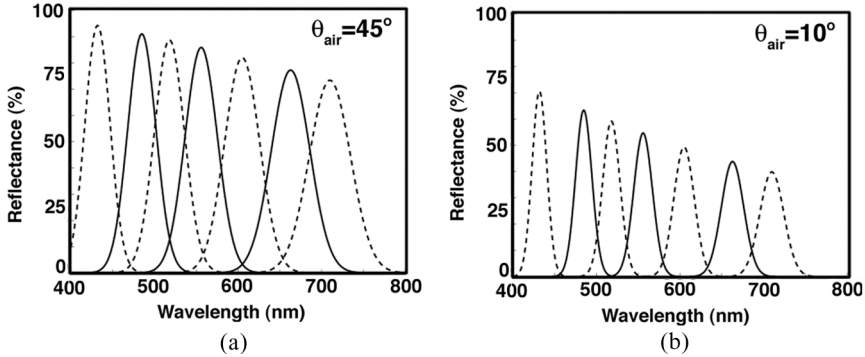

FIGURE 4 Modeled reflection spectra of a VA-DHFLC at 45 degree incidence (a) and 5 degree incidence (b).

wavelength as a function of temperature for the VA-DHFLC cell, closely following the quadratic correlation shown. In the short wavelength visible spectrum (peak at 420 nm), the VA-DHFLC shows a peak reflectivity of 75% for unpolarized light. Shifting to the long wavelength visible regime, the peak reflectivity decreases to 50% (peak at 710 nm) as a result of the decreased number of Bragg planes for longer wavelength light before losing all selective reflectivity beyond the nematic* phase transition temperature at 83°C. Reflectivity and thus sensitivity is maximized in the high incidence angle ($\theta_{\text{air}} = 45^{\circ}$) alignment. In this configuration, the FWHM in short wavelength visible regime is $\sim$25 nm and broadens to $\sim$45 nm in the long wavelength visible regime. The shift in reflection characteristics as a function of peak reflection wavelength is in agreement with the modeled reflection spectra as are shown in Figure 4(a). The tunable Bragg grating model shows a similar decrease in reflection efficiency and increase in bandwidth with increasing λ_0. The modeled results have a peak reflectivity of 94% and FWHM of 35 nm at the short wavelength visible peak (420 nm) and a peak reflectivity of 73% and FWHM of 60 nm at the long wavelength visible peak (710 nm) using an index modulation of 0.058 estimated using Eq. (4) with $\theta_{\text{air}} = 45^{\circ}$ ($\theta_{\text{inc}} = 28.1^{\circ}$), $\theta_{\text{tilt}} = 38^{\circ}$, and cell thickness, d, of 10 μm. The increased peak reflectivity and increased bandwidth for the modeled system compared to the experimental system can likely be attributed to the model assumption of perfect alignment of the Bragg planes along the incidence wavevector. Alignment imperfection decreases the total index modulation experienced and has the effect of lowering the peak reflectivity as well as the bandwidth, as is the case here. Figure 4(b) is

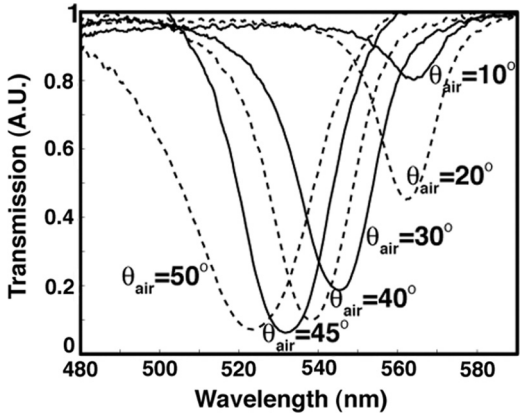

FIGURE 5 Variation of bandwidth and efficiency of transmission spectra as a function of incidence angle.

the modeled reflection notch characteristics with an incidence angle $\theta_{air} = 10^{\circ}$, a significant improvement in notch bandwidth and resultant resolution as compared to the modeled reflection notch characteristics with incidence angle $\theta_{air} = 45^{\circ}$ as shown in Figure 4(a). At $\theta_{air} = 10^{\circ}$, the FWHM = 18 nm at a short wavelength visible peak (420 nm) and FWHM = 30 nm at a long wavelength visible peak (710 nm) with a calculated index modulation of 0.036.

As shown in Figure 4, the incidence angle is of particular importance in designing the microspectrometer as the resolution and sensitivity are directly correlated to the index modulation and thus the operating incidence angle. Figure 5 shows the experimentally measured VA-DHFLC transmission spectra as a function of incidence angle in air. At a low incidence angle $\theta_{air} = 10^{\circ}$ ($\theta_{inc} = 6.8^{\circ}$), the FWHM is 14 nm. As the incidence angle is increased to $\theta_{air} = 50^{\circ}$ ($\theta_{inc} = 28.1^{\circ}$), the reflection bandwidth increases to 35 nm as a result of increased index modulation. The slight drop in reflection intensity from $\theta_{air} = 45^{\circ}$ to $\theta_{air} = 50^{\circ}$ is likely the result of initial waveguide losses in substrates as the continued broadening transmission notch suggests the effective birefringence is continuing to increase as the model predicts.

Figure 6 shows the reflected intensity for right handed and left handed circularly polarized light (the two spectra are offset for clarity). The variation in the peak reflected laser intensity is 1.3% between the two orthogonal polarization states, showing that the VA-DHFLC is mostly polarization insensitive more analogous to an

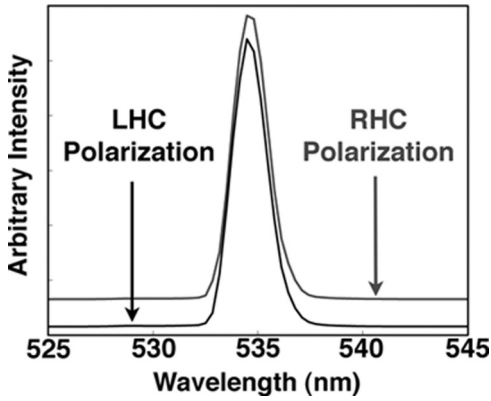

FIGURE 6 Reflection intensity of a 532 nm Argon-ion laser with left-hand and right-hand circular polarization (Offset for clarity).

H-PDLC as opposed to a CLC. This allows a microspectrometer based on this technology to be inherently more simple and sensitive by not requiring one filter for each circular polarization.

4.2. Spectrometer Performance

The emission spectra of an the mercury arc lamp as measured by a grating spectrometer and as determined both theoretically and experimentally using a VA-DHFLC microspectrometer are shown in Figure (7) while the same is shown for an LCD in Figure (8). Although the loss in resolution is present from a commercial fiber based spectrometer to the LC system, analogous spectral features between data are clearly observable. The modeled spectral signatures are in good agreement with experimentally determined signatures, although particularly in the case of the mercury lamp, the experimentally measured signature has improved resolution. The peak in the mercury spectrum at 436 nm has an experimentally determined FWHM of 15 nm using the VA-DHFLC operating at $\theta_{\text{air}} = 25^{\circ}$ and a model determined FWHM of 23 nm with the same parameters. This is a result of the discrepancy in ideal modeled effective birefringence as opposed to actual effective birefringence narrowing the peak linewidth and thus features linewidth as explained previously. Both experimental and theoretical spectra demonstrate this device is capable of resolving the doublet in the mercury spectra at 546 nm and 579 nm. The recreated LCD emission spectra show that the VA-DHFLC device

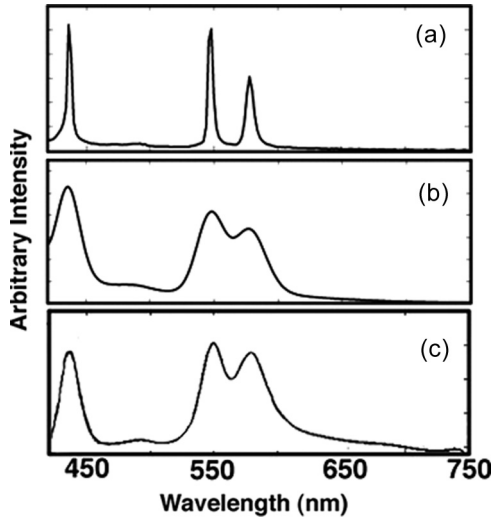

FIGURE 7 Emission spectrum of a mercury lamp measured using a grating spectrometer (a), modeled VA-DHFLC performance (b), and fabricated VA-DHFLC (c).

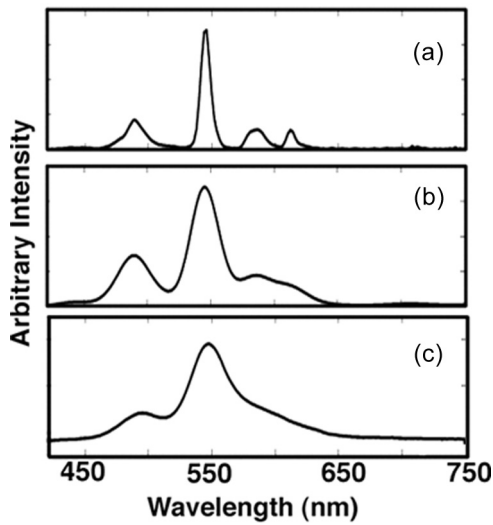

FIGURE 8 Emission spectrum of green pixels of an LCD measured using a grating spectrometer (a), modeled VA-DHFLC performance (b), and fabricated VA-DHFLC (c).

is also suitable in monitoring broadband spectral lineshapes as opposed to narrow emission lines, as is the case in several spectroscopy applications.

5. DISCUSSION

As shown in Figure 3, the thermally tuned VA-DHFLC device with this FLC material has a dynamic range of 450 nm to 750 nm. The upper threshold is defined for thermally tuned devices by the FLC-nematic* phase transition point after which the FLC no longer maintains is helical structure. The dynamic range of a thermally tunable cell can be shifted to longer wavelengths and near-infrared by integrating an FLC material with a longer resting (room temperature) helical pitch such that the window of tunable reflection wavelengths is shifted for temperatures in the smectic C* phase. An electrically controllable cell with patterned ITO has a larger dynamic range as the phase transition does not sharply limit the upper bound; however, the upper bound is limited by the reduced number of Bragg planes at long wavelength helical pitches causing a decrease in the peak reflectivity (see Eq. (5) where λ_0 is increasing and d remains constant). A tunable FLC NIR spectroscope is most effectively fabricated using a thermally tuning VA-DHFLC cell using longer pitch FLC materials and a thick VA-DHFLC cell gap to assure numerous Bragg planes even at the upper limit of the device dynamic range. These thick cells must be thermally addressed because of the inability of feasible electric fields to effectively deform the helical pitch uniformly though the larger cell gap.

The VA-DHFLC microspectrometer is an enabling technology for numerous applications. The size and cost of these devices enables online rapid colorimetry, gas and liquid analysis for quality control/screening applications. Integration of a microspectrometer into a MEMS system such as a microfluidics chip can enhance functionality of these systems, namely spectral mapping of single channels in approximate real time. One particular application of particular interest is the use of a VA-DHFLC as microspectrometers in noninvasive optical diagnostic tools as we have highlighted elsewhere [21]. The narrow band reflection spectrum and full spectrum tunability of a single panel also enable the VA-DHFLC to be integrated into a miniature spectral imaging device as opposed to a single pixel microspectrometer. Adding spectral imaging capabilities to the VA-DHFLC requires integration of a Grayscale CCD detector with high sensitivity and additional focus on the spatial uniformity of DHFLC cell to assure uniformity of spectral signals at the image plane. Tuning the VA-DHFLC

into the NIR and fabricating a handheld inexpensive NIR imaging device has tremendous potential in a number of noninvasive medical imaging application, including mammography and dermatology.

One distinct advantage of a narrow band ferroelectric liquid crystal notch filter is the potential fast response times when driving this device in the in-plane switching electric field mode. As a result of the spontaneous polarization in a ferroelectric liquid crystal, the orientation of the ferroelectric liquid crystal couples to the applied field polarity, allowing electric field to drive the helix to wind and unwind causing the respective blue-shift and red-shift. Unlike nematic liquid crystal which require an induced dipole moment and are insensitive to the electric field polarity, the permanent dipole in an FLC has shown switching times of 2 ms in a light valve display configuration switching the entire helix on a cone [17]. As a VA-DHFLC microspectrometer utilizes the intermediate unwinding states of the helix, shorter switching times are hypothesized as the helix has less deformation (although yet to be experimentally verified). The narrow band and fast switching time of a VA-DHFLC make this device a potential choice for spectral discrimination elements in two fluorophore scanning microscopy, particularly when the two fluorophore signals need to be co-localized on a single FPA. Using a single FPA and rapidly switchable filter for discerning fluorescent markers, fluorescently tagged areas can be co-localized and dynamics can be observed in close to real time.

6. CONCLUSIONS

A VA-DHFLC microspectrometer has been fabricated using homeotropically aligned ferroelectric liquid crystal and a single pixel photodiode. This device can be tuned with a narrow reflection notch fully through the visible spectra regime using thermal modulation. The reflection notch characteristics were investigated both experimentally measured reflection spectra and modeled reflection spectra treating the VA-DHFLC as a tunable Bragg reflection grating and estimating the effective birefringence through the geometrical configuration. Performance tests involving emission spectra from a liquid crystal display have demonstrated the feasibility and resolution of a microspectrometer created with a single vertically aligned deformed helix ferroelectric liquid crystal and a single pixel photodiode. A DHFLC based spectrometer is advantageous over other reported methods of fabricating microspectrometers as it only requires two components for operation, does not depend on high resolution focal plane arrays for wavelength resolution, and is straightforward to fabricate and align.

While the inexpensive nature of a DHFLC microspectrometer allows it to replace more expensive and bulky spectrometers in rapid and routine screening applications, the ultra-compact aspect of this device enables new applications of spectral analysis where prior instrumentation has limited functionality. A survey of existing applications potentially impacted by an inexpensive microspectrometer includes handheld optical diagnostic devices, spectrochemical analysis, and MEMS devices.

REFERENCES

[1] Correia, J. H., de Graaf, G., Kong, S. H., Bartek, M., & Wolffenbuttel, R. F. (2000). *Sensors and Actuators a-Physical*, *82*, 191.
[2] Lammel, G., Schweizer, S., & Renaud, P. (2001). *Sensors and Actuators a-Physical*, *92*, 52.
[3] Boer, G., Ruffieux, P., Scharf, T., Seitz, P., & Dandliker, R. (2004). *Applied Optics*, *43*, 2201.
[4] Collins, S. D., Smith, R. L., Gonzalez, C., Stewart, K. P., Hagopian, J. G., & Sirota, J. M. (1999). *Optics Letters*, *24*, 844.
[5] Manzardo, O., Herzig, H. P., Marxer, C. R., & de Rooij, N. F. (1999). *Optics Letters*, *24*, 1705.
[6] Padgett, M. J., Harvey, A. R., Duncan, A. J., & Sibbett, W. (1994). *Applied Optics*, *33*, 6035.
[7] Sander, D. & Muller, J. (2001). *Sensors and Actuators a-Physical*, *88*, 1.
[8] Brennan, D., Alderman, J., Sattler, L., Walshe, J., Huang, J., O'Connor, B., & O'Mathuna, C. (2002). *Infrared Physics & Technology*, *43*, 69.
[9] Yang, D. K., Huang, X. Y., & Zhu, Y. M. (1997). *Annual Review of Materials Science*, *27*, 117.
[10] Xianyu, H. Q., Faris, S., & Crawford, G. P. (2004). *Applied Optics*, *43*, 5006.
[11] Date, M., Takeuchi, Y., & Kato, K. (1998). *Journal of Physics D-Applied Physics*, *31*, 2225.
[12] Fiske, T. G., Silverstein, L. D., Colegrove, J., & Yuan, H. (2000). *SID International Symposium Digest of Technical Papers*, *31*, 1134.
[13] Kim, H. R., Lee, Y. W., Kim, S. J., Kim, D. W., Yu, C. J., Lee, B., & Lee, S. D. (2004). *Ferroelectrics*, *312*, 479.
[14] Ozaki, M., Kasano, M., Ganzke, D., Haase, W., & Yoshino, K. (2002). *Advanced Materials*, *14*, 306.
[15] Choi, W. K., Davey, A. B., Wilkinson, T. D., & Crossland, W. A. (1997). *Molecular Crystals and Liquid Crystals Science and Technology Section A-Molecular Crystals and Liquid Crystals*, *304*, 329.
[16] Cohen, A. D., Parker, M. C., & Mears, R. J. (1998). *Ferroelectrics*, *214*, 775.
[17] You, D. H., Yu, C. J., & Lee, S. D. (2002). *Ferroelectrics*, *278*, 805.
[18] Pozhidaev, E. P., Smorgon, S. L., Andreev, A. L., Kompanets, I. N., Zyryanov, V. Y., & Kompanets, S. I. (1998). *Ferroelectrics*, *212*, 153.
[19] Smorgon, S. L., Barannik, A. V., Zyryanov, V. Y., Pozhidaev, E. P., Andreev, A. L., Kompanets, I. N., Ganzke, D., & Haase, W. (2001). *Molecular Crystals and Liquid Crystals*, *368*, 3975.
[20] Hariharan, P. (1996). *Optical Holography: Principles, Techniques and Applications*, Cambridge University Press: Sydney, Australia.
[21] McMurdy, J. W., Jay, G. D., Suner, S., Trespalacios, F. M., & Crawford, G. P. (2006). *Journal of Biomedical Optics*, *11*, 014019.